


Neural stem cells in the adult olfactory bulb core generate mature neurons in vivo

Çağla Defterali^{1,2} | Mireia Moreno-Estellés^{3,4} | Carlos Crespo⁵ |
 Eva Díaz-Guerra^{1,2} | María Díaz-Moreno³ | Eva Vergaño-Vera^{1,2} |
 Vanesa Nieto-Estévez^{1,2} | Anahí Hurtado-Chong^{1,2} | Antonella Consiglio^{6,7} |
 Helena Mira^{3,4} | Carlos Vicario^{1,2} 

¹Instituto Cajal-Consejo Superior de Investigaciones Científicas (CSIC), Madrid, Spain

²CIBERNED-Instituto de Salud Carlos III (ISCIII), Madrid, Spain

³Unidad de Neurobiología Molecular, Área de Biología Celular y del Desarrollo, CNM-ISCIII, Majadahonda, Spain

⁴Instituto de Biomedicina de Valencia-CSIC (IBV-CSIC), Valencia, Spain

⁵Departamento de Biología Celular, Estructura de Investigación Interdisciplinar en Biotecnología y Biomedicina (BIOTECMED), Universitat de Valencia, Valencia, Spain

⁶Institute of Biomedicine, Department of Pathology and Experimental Therapeutics, Bellvitge University Hospital-IDIBELL, Barcelona, Spain

⁷Department of Molecular and Translational Medicine, University of Brescia, Brescia, Italy

Correspondence

Carlos Vicario, PhD, Instituto Cajal-CSIC, Avenida Doctor Arce 37, E-28002 Madrid, Spain. Email: cvicario@cajal.csic.es

Funding information

Comunidad de Madrid, Grant/Award Number: S2011/BMD-2336; Consejo Superior de Investigaciones Científicas, Grant/Award Numbers: 201220E098, 201320E054; Generalitat Valenciana, Grant/Award Number: PROMETEO/2018/055; Instituto de Salud Carlos III, Grant/Award Numbers: CIBERNED CB06/05/0065, RD16/0011/0024, PIE14/00061; Secretaría de Estado de Investigación, Desarrollo e Innovación, Grant/Award Numbers: BFU2016-80870-P, SAF2013-4759R, SAF2016-80419-R, PID2019-109059RB-I00, SAF2015-70433-R

Abstract

Although previous studies suggest that neural stem cells (NSCs) exist in the adult olfactory bulb (OB), their location, identity, and capacity to generate mature neurons in vivo has been little explored. Here, we injected enhanced green fluorescent protein (EGFP)-expressing retroviral particles into the OB core of adult mice to label dividing cells and to track the differentiation/maturation of any neurons they might generate. EGFP-labeled cells initially expressed adult NSC markers on days 1 to 3 postinjection (dpi), including Nestin, GLAST, Sox2, Prominin-1, and GFAP. EGFP⁺-doublecortin (DCX) cells with a migratory morphology were also detected and their abundance increased over a 7-day period. Furthermore, EGFP-labeled cells progressively became NeuN⁺ neurons, they acquired neuronal morphologies, and they became immunoreactive for OB neuron subtype markers, the most abundant representing calretinin expressing interneurons. OB-NSCs also generated glial cells, suggesting they could be multipotent in vivo. Significantly, the newly generated neurons established and received synaptic contacts, and they expressed presynaptic proteins and the transcription factor pCREB. By contrast, when the retroviral particles were injected into the subventricular zone (SVZ), nearly all (98%) EGFP⁺-cells were postmitotic when they reached the OB core, implying that the vast majority of proliferating cells present in the OB are not derived from the SVZ. Furthermore, we detected slowly dividing label-retaining cells in this region that could correspond to the population of resident NSCs. This is the first time NSCs located in the adult OB core have been shown to generate neurons that incorporate into OB circuits in vivo.

KEYWORDS

adult neurogenesis, calretinin, interneurons, neural stem cells, olfactory bulb, synapses

This is an open access article under the terms of the Creative Commons Attribution-NonCommercial License, which permits use, distribution and reproduction in any medium, provided the original work is properly cited and is not used for commercial purposes.

© 2021 The Authors. STEM CELLS published by Wiley Periodicals LLC on behalf of AlphaMed Press.

1 | INTRODUCTION

Neuroblasts are continuously born from neural stem cells (NSCs) (also known as type B1 cells) in the mouse ventricular-subventricular zone (V-SVZ) of the postnatal lateral ventricle. These neuroblasts migrate tangentially along the radial migratory stream (RMS) toward the olfactory bulb (OB), where they subsequently migrate radially and differentiate into multiple types of neurons.¹⁻⁷ The majority of newly formed neurons will ultimately end up in the granular cell layer (GCL) or glomerular layer (GL), and they will mature into specific subtypes of GABAergic and dopaminergic OB interneurons, all of which are inhibitory.⁸⁻¹³ However, a very small number of Tbr2⁺ glutamatergic juxtglomerular neurons are also generated from SVZ NSCs and they end up in the external plexiform layer (EPL).¹⁴ Indeed, type B1 cells are heterogeneous and they generate different types of interneurons, ultimately derived from finely patterned SVZ subdomains.^{9,15} In the OB, nonoverlapping interneuron subpopulations can be distinguished on the basis of their location, morphology, connectivity, and molecular markers, such as the calcium binding proteins calretinin (Calr), calbindin (Calb), and parvalbumin (PVA).^{9,16-22}

Although the SVZ is the main source of OB interneurons, a number of studies claimed local NSCs exist in the adult rodent and human OB.²³⁻³¹ Furthermore, it has been reported that cells derived from the human OB give rise to neurons and glia in cell culture.³²⁻³⁷ However, the precise location, features, and most importantly, the full neurogenic potential of these NSCs *in vivo* has yet to be defined.

In the light of the above, we herein describe the use of retroviral injections to characterize the dividing cells in the OB core and their progeny *in vivo*. Following the injections, the cell's molecular markers were analyzed, as were their morphology and connectivity (by electron microscopy [EM]). Our results show that NSCs in the OB core predominantly give rise to Calr⁺ interneurons, with other cell types significantly less abundant. Moreover, we show for the first time that the locally formed neurons establish synapses and express synaptic-related proteins, suggesting they incorporate into the OB circuitry.

2 | MATERIALS AND METHODS

2.1 | Animals

All animal care and handling was carried out in accordance with European Union guidelines (directive 2010/63/EU) and Spanish legislation (Law 32/2007 and RD 53/2013). All the protocols were approved by the Ethics Committees of the Consejo Superior de Investigaciones Científicas (CSIC, Madrid), the Comunidad de Madrid and the University of Barcelona.

2.2 | Injection of retroviral vectors into the adult OB and SVZ, perfusion, and immunohistochemistry

Injections were performed on 9-week-old wild-type C57BL/6N mice using a digital stereotaxic instrument. The pRV-EGFP vector was

Significance statement

The adult olfactory bulb (OB) receives neurons originating from the subventricular zone and from the elbow of the rostral migratory stream but it remains unclear whether local neural stem cells (NSCs) contribute to neurogenesis in the OB. The results of this study show for the first time that NSCs in the adult OB core predominantly give rise to calretinin-expressing interneurons. Notably, not only do the newly generated neurons establish synapses but they also express synaptic proteins and pCREB *in vivo*, indicating they become incorporated into the OB's synaptic circuits.

injected into the left OB core along with polybrene (2.5 μ L) at the coordinates (anteroposterior to bregma +5.1 mm, lateral to midline \pm 0.8 mm, ventral to dura -1.1 mm).³⁰

The animals were anesthetized on day 1, 2, 3, 7, and 21 post-injection (pi) with an intraperitoneal (ip) pentobarbital and then, perfused transcardially with 0.9% NaCl followed by 4% paraformaldehyde (PFA). The animal's brain was postfixed for 48 hours, embedded in 3% agarose, and serial coronal 30- to 50- μ m vibratome sections were obtained and processed for immunohistochemistry using antibodies against to cell-type and/or cell stage specific markers ("Extended Materials and Methods" section in Supporting Information). Sections were always costained with a GFP antibody, thus allowing unambiguous visualization and examination of EGFP-labeled cells even at early dpi.

2.3 | EM analysis of EGFP⁺ cells

The injected animals were processed and the EGFP⁺ cells were analyzed by EM at 28 dpi to assess the synaptic connectivity of the newly generated neurons ("Extended Materials and Methods" section in Supporting Information).

2.4 | Injections of lentiviral vectors into the adult OB and SVZ, and preparation of neurosphere cultures from the injected and noninjected regions

One microliter of lentiviral (LV) vector was stereotaxically injected in the OB and in the SVZ (AP + 0.8, ML -1.3, DV -2.5) of 8-week-old C57/BL6 mice. One day before the LV injections were performed, a group of six animals received three intraperitoneal injections of 5-chloro-2-deoxyuridine (CldU, 50 mg/kg) every 2 hours to identify the potential label-retaining cell (LRC) population. Serial coronal vibratome sections of the OB (40 μ m) were immunostained with specific antibodies ("Extended Materials and Methods" section in Supporting Information). Neurosphere cultures were prepared as reported previously.²⁹

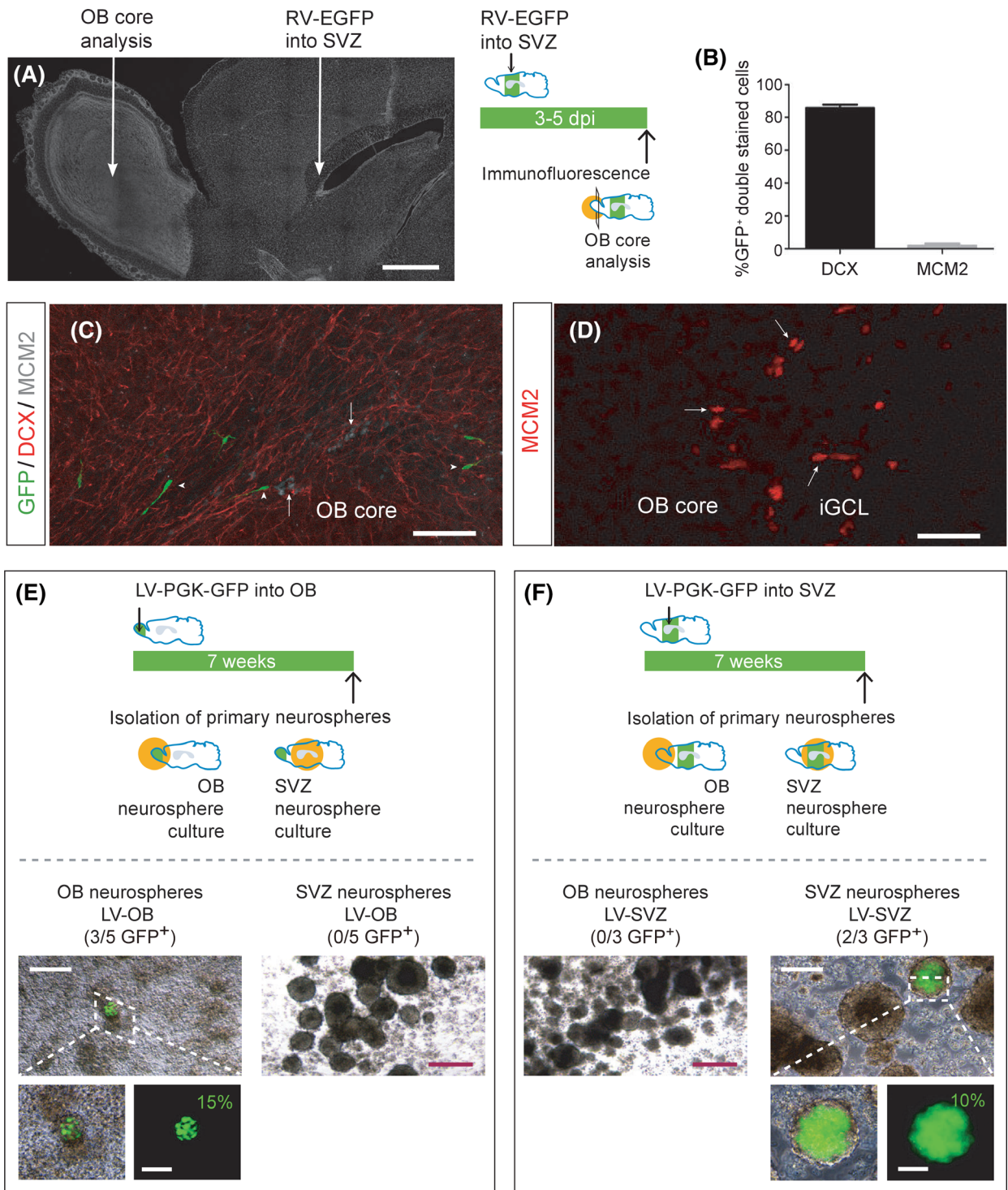


FIGURE 1 The large majority of neural progenitor cells from the adult mouse SVZ stop dividing before reaching the OB core and do not contribute to primary neurosphere formation from dissected OB tissue. A, Experimental design of the SVZ retroviral labeling. An EGFP-expressing retroviral vector (RV-EGFP) was injected into the SVZ of 9-week-old mice and the OB was then analyzed by immunohistochemistry. EGFP-labeled cells were only detected in the OB core at 3, 4, and 5 days postinjection (dpi). B, Of the EGFP+ cells in the OB, 83.3% were labeled for DCX while only 1.9% were positive for MCM2. C, All EGFP+DCX+ cells that reached the OB from the SVZ were devoid of MCM2 (arrowheads). D, By contrast, cells located in the OB core were immunolabeled with MCM2 antibody [arrows in (C) and (D)]. E,F, Two-month-old animals were injected with a green fluorescent protein-expressing lentiviral vector (LV-PGK-GFP) vector into the OB (E; n = 5, LV-OB group) or the SVZ (F; n = 3, LV-SVZ group) and were sacrificed 7 weeks later. In LV-OB animals (E), GFP+ neurospheres were obtained only from the OB (in three out of five independent animals, 3/5; 15% of the spheres were GFP+). In LV-SVZ animals (F), GFP+ neurospheres were obtained only from the SVZ (2/3; 10% of the spheres were GFP+). Scale bars = 925.9 μm (A); 77.6 μm (C); 20.7 μm (D). Scale bars in (E, F) = 100 μm (upper panels images containing GFP+ neurospheres), 200 μm (images containing no GFP+ neurospheres), 50 μm (magnifications of GFP+ neurospheres, below). DCX, doublecortin; OB, olfactory bulb; RV-EGFP, retroviral particles expressing EGFP; SVZ, subventricular zone

2.5 | Quantitative and statistical analyses

In the mice injected with the EGFP retroviral vector, photos of all EGFP⁺ cells were taken from each section and the colocalization of specific markers with the GFP antibody was analyzed. To capture the whole section, individual z-planes at a resolution of 1024 × 1024 were examined every 2 μm with a ×20 objective. If necessary, a ×63 objective was used to pinpoint double staining at a zoom of x2-3. The entire z-stack of the whole section or of the OB core was counted to calculate the number of GFP⁺ cells and colocalization with the GFP marker was analyzed in each individual plane of each section using ImageJ. Results in Figure 3G are shown as the mean (±SEM) of total GFP⁺ cells per volume, which was determined using the ImageJ software on confocal z-stacks. For all the experiments, sections from three to five animals per condition (“n” value) were examined.

An unpaired two-tailed Student's *t* test was used to compare the mean ± SEM values from two experimental conditions, with a Welch's correction when the *F* test indicated significant differences between the variances of both groups. Statistical analyses compared more than two experimental conditions using one-way analysis of variance (ANOVA) and Kruskal-Wallis tests. For parametric distributions and equal variances measured by Barlett's test, one-way ANOVA was used with Tukey's post hoc test. When the variances were not equal (as measured by a Barlett's test), a nonparametric Kruskal-Wallis test was used with a post hoc Dunn's test. Statistical significance was set at **P* < .05 and GraphPad Prism 5.0 was used for all statistical analyses.

In the mice injected with LV particles (n = 3-5 mice per condition), individual confocal microscope (Leica) images were taken in the z-plane every 2 μm and the EGFP⁺ cells were counted using the LAS AF Lite software (Leica). Statistical analysis was carried out using an unpaired two-tailed Student's *t* test after determining that the data followed a normal distribution using the Kolmogorov-Smirnov test and assessing the equality of variances with the Levene test. Statistical significance was set at *P* < .05.

3 | RESULTS

3.1 | The adult OB core contains dividing cells that do not originate in the SVZ

Using retroviral labeling, we aimed to study whether new synaptically mature neurons can be generated from dividing neural progenitors present in the adult mouse OB core. To achieve this, it was critical to first investigate whether SVZ-derived cells² that migrate through the RMS were still dividing or not by the time they reach the OB core (see Figures 1A, 2F,G, and S1), and hence, we injected retroviral particles expressing EGFP (RV-EGFP, which only infects dividing cells) into the SVZ of adult mice (Figure 1A). When the injected animals were analyzed 1 to 5 dpi, EGFP-labeled cells could only be clearly detected in the OB core at 3, 4, and 5 dpi.

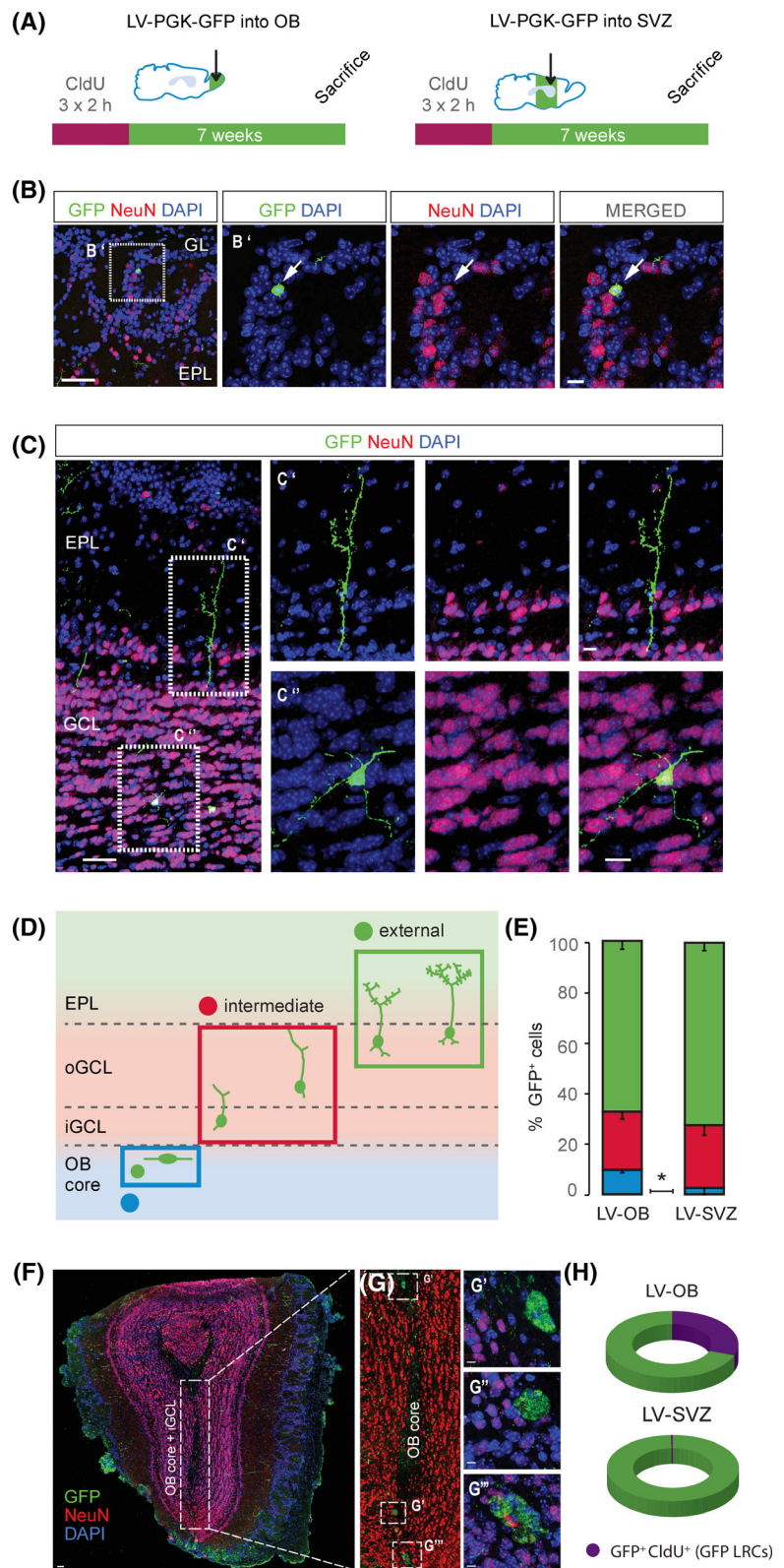
Importantly, a key study described that the majority of cells labeled with [³H] Thymidine in the SVZ were found in the OB GCL and GL at 15 dpi.⁵ Thus, we focused on the 3 to 5 dpi time points for further analysis, as they represent the days when more SVZ-derived cells reach the OB core, our area of interest. We immunostained the labeled cells using antibodies against GFP, DCX (a marker of neuroblasts and immature neurons), and MCM2 (a marker of dividing cells).^{38,39} As seen in Figure 1B, 83.3% of the EGFP⁺ cells expressed DCX, whereas only 1.92% of the EGFP⁺ cells were labeled for MCM2. Furthermore, all the migrating EGFP⁺DCX⁺ cells that reach the OB from the SVZ were devoid of MCM2 in the OB (Figure 1C), indicating that they do not divide in this structure. We obtained a lower proportion of dividing EGFP⁺ cells when assessed with an anti-Ki67 antibody (0.76%, n = 5). Importantly, MCM2⁺ cells were present in the OB core and in the surrounding inner GCL (iGCL) (Figure 1D). Therefore, our data demonstrate that almost all (98%-99%) the SVZ-derived cells do not proliferate in the OB core, indicating that the vast majority of dividing cells detected in the OB core are not derived from the SVZ.

To extend these findings, we injected LV-PGK-GFP lentiviral particles into the OB core or into the SVZ of 8- to 9-week-old mice, and we performed a primary neurosphere formation assay 7 weeks later, both on the OB and the SVZ dissected tissue (Figure 1E). GFP-labeled primary neurospheres (15%) formed in cultures derived from the injected OB (in three out of five injected animals) but not in cultures from the noninjected SVZ (0/5) of the same animals. The opposite was found when the LV particles were injected into the SVZ (Figure 1F), with GFP-positive primary neurospheres (10%) formed in cultures from the injected SVZ (2/3) but not in those from the OB (0/3). The neurospheres derived from the OB appeared to be smaller than those derived from the SVZ, in line with a previous study.²⁹ Together, these results show that neurosphere forming cells located in the OB are not derived from the SVZ, and concur with the existence of a local pool of NSCs in the OB.^{23,26,28,29}

3.2 | The adult OB core cells include LRCs

To assess if the dividing cells found in the adult OB core correspond to local slowly dividing LRCs that could be the source of the primary neurospheres, we administered CldU (which incorporates into the DNA of dividing cells) to 2-month-old animals the day after injecting the LV-PGK-GFP vector, which infects both dividing and nondividing cells. The GFP-expressing LV particles were injected either into the OB core (LV-OB animals) or into the SVZ (LV-SVZ animals) and after 7 weeks, the OB was analyzed by immunofluorescence (Figure 2A). In both sets of mice, GFP⁺NeuN⁺ cells were found outside the OB core, in the GL and GCL (Figure 2B-D), yet the proportion of GFP⁺ cells in the OB core of LV-OB animals was almost three times higher than in LV-SVZ animals (*P* = .036, unpaired Student's *t* test, Figure 2E). Moreover, in the OB core of some LV-OB mice, the GFP⁺NeuN⁻ cells formed small clusters of globular cells (Figure 2F, G). In addition, 30.6% ± 9.2% of GFP⁺ cells in the OB core of LV-OB

FIGURE 2 Label-retaining cells (LRCs) persist in the adult OB core. A, Experimental design of the LRC and lentiviral labeling protocol. CldU was injected i.p. into 2-month-old mice and the next day, LV-PGK-GFP particles were injected into either the OB core (LV-OB animals) or the SVZ (LV-SVZ animals). The OB was analyzed by immunofluorescence 7 weeks later. B, Representative image of a GFP⁺NeuN⁺ neuron in the glomerular layer (GL) of an LV-OB animal (arrow). B', Magnifications of the area shown in (B). C, Representative images of GFP⁺NeuN⁺ neurons found in the granule cell layer (GCL) of LV-OB animals. C', C'', Magnifications of the areas shown in (C). D, E, Seven weeks after LV injection, the percentage of GFP⁺ cells in the OB core of LV-OB animals was almost three times higher than in LV-SVZ animals (**P* = .036, unpaired Student's *t* test). F, Representative image of an OB section from a mouse injected with the LV-PGK-GFP vector into the OB core and immunostained with an anti-NeuN antibody. G, Clusters of GFP⁺ cells that did not stain for the neuronal marker NeuN (putative NSCs) were detected at restricted sites in the OB core. G', G'', G''', Magnifications of the areas shown in G. H, Percentage of GFP⁺ cells in the OB core of LV-OB animals that were labeled with CldU (GFP⁺ LRCs, purple). No GFP⁺ LRCs were found in LV-SVZ animals. Scale bars in (B, C): 10 μm; (B' and C', C'' high magnifications): 5 μm; (F): 100 μm; (G): 50 μm; (G', G'', G'''): 5 μm. CldU, 5-chloro-2-deoxyuridine; GCL, granular cell layer; GL, glomerular layer; LV-OB, lentiviral olfactory bulb; NSCs, neural stem cells; OB, olfactory bulb; SVZ, subventricular zone



animals incorporated CldU (GFP⁺ LRCs, Figure 2H), whereas such double labeled cells (GFP⁺CldU⁺) were never found in the OB core of LV-SVZ animals. Although the genetic strategy may affect the

results of this experiment, our findings suggest that slowly dividing LRCs exist in the adult OB core that possibly correspond to a population of resident NSCs.

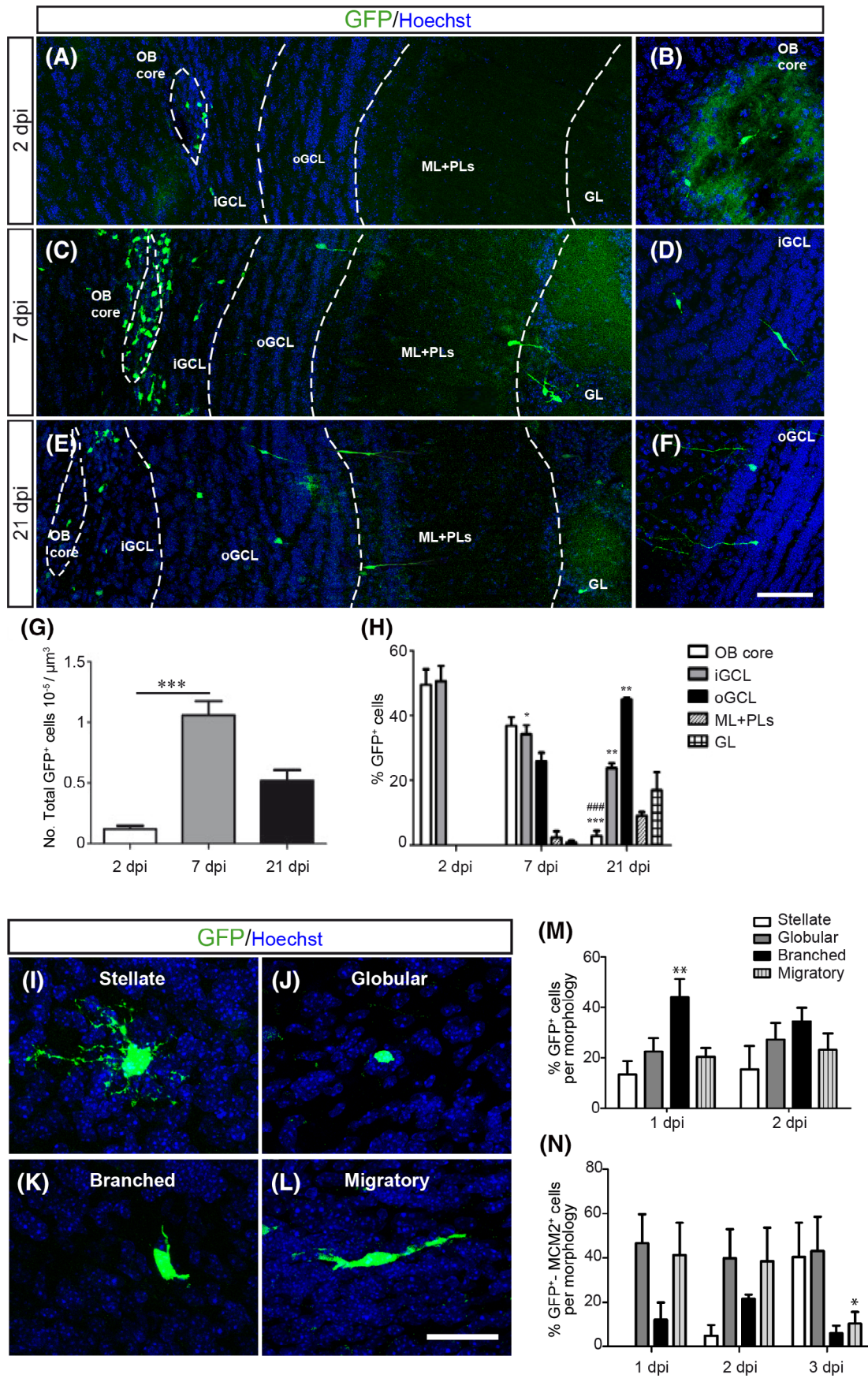


FIGURE 3 Legend on next page.

3.3 | Characterization of the dividing cells and their progeny in the adult OB

3.3.1 | The progeny of dividing cells migrate out of the OB core and differentiate into neurons

As indicated above, SVZ-derived cells do not appear to proliferate in the OB, implying that the vast majority of SVZ cells that reach the OB will not be labeled by retroviral particles injected into the OB core. This allows us to explore local OB neurogenesis using a retroviral lineage tracing approach together with immunohistochemistry, coupled to morphological and EM analyses.³⁰ The RV-EGFP vector was focally injected into the OB core (Figure S1) and the animals were analyzed at 1, 2, 3, 7, 21, and 28 dpi (Figures 3-7 and S2-S5). This focal injection minimizes a potential retrograde virus spreading in the RMS elbow, a region containing NSCs that predominantly generate OB dopaminergic interneurons in addition to granule cells.⁴⁰⁻⁴⁴

The cells labeled with the RV-EGFP vector were detected by immunostaining against GFP, and their general morphology and distribution in the different OB layers was assessed at 2, 7, and 21 dpi after counterstaining their nuclei with Hoechst (Figure 3A-F). A significant, sixfold increase in the number of EGFP⁺-cells was seen between 2 and 7 dpi ($***P = .0001$, one-way ANOVA with Tukey's post hoc test; Figure 3G). At 7 dpi, the total number of labeled cells reached its maximum. At 2 dpi, all the labeled cells were found in the OB core (49.5%) and iGCL (50.5%; Figure 3A,B,H). While at 7 dpi, the majority of cells still remained within the OB core (36.8%) and iGCL (34.2%; $*P = .034$, one-way ANOVA followed by Tukey's post hoc test, 7 dpi vs 2 dpi), a proportion of cells began to migrate out of this region, with 25.8% of the cells detected in the outer GCL (oGCL) and a few EGFP-labeled

cells reaching the mitral (ML) and plexiform (PL) layers (2.4%) or the GL (0.8%; Figure 3C,D,H). By 21 dpi, few cells (2.8%) persisted in the OB core relative to 2 dpi ($***P = .0001$, one-way ANOVA followed by Tukey's post hoc test) and 7 dpi ($###P = .0001$, one-way ANOVA with Tukey's post hoc test), whereas 23.7% of cells were in the iGCL ($**P = .0034$, one-way ANOVA followed by Tukey's post hoc test, 21 dpi vs 2 dpi). By this stage most of the cells had migrated to the oGCL (44.9%; $**P = .0023$, unpaired *t* test, two-tailed, *df* = 4, *t* = 6.946; 21 dpi vs 7 dpi), the ML and PL (9%), or the GL (16.9%, Figure 3E,F,H). However, we did not observe a regional bias regarding the final location of interneurons toward the medial or lateral OB. The morphology of the cells reflected their very immature state at 2 dpi, mostly round or globular cells bearing a small process (Figure 3A,B). However, at 7 and 21 dpi the majority of cells adopted a morphology reminiscent of migratory neuroblasts with a single well-developed leading process, that of differentiated granule neurons with an apical dendrite and various short dendrites or of periglomerular neurons (Figure 3C-F).

3.3.2 | Characterization of progenitor cells in the adult OB core suggests the existence of local NSCs and committed progenitors

To characterize the neural progenitors existing in the OB core *in vivo*, we extended our study and performed a comprehensive morphological analysis (Figure 3I-N) and a molecular analysis (Figures 4 and S2) at early time points after injection (1-3 dpi), when EGFP-labeled cells are more abundant in the OB core (Figure 3A,H). The first analysis identified four different morphologies of EGFP-labeled cells (Figure 3I-L): stellate cells with a polygonal cell body bearing numerous processes;

FIGURE 3 The distribution of EGFP⁺ labeled cells in the adult OB is indicative of the migration and differentiation of newly generated neurons from dividing NSCs and neural progenitors located in the OB core. A-H, An enhanced green fluorescent protein (EGFP)-expressing retroviral vector was injected into the adult OB core in order to label proliferative cells and their progeny in the different neuronal layers of the OB. The images show the distribution of EGFP-labeled cells at 2 (A), 7 (C), and 21 days postinjection (dpi) (E), and high magnification images of cells at each time point, respectively (B, D, F). The cells adopted a very immature morphology at 2 dpi and most of them were apparently round or globular in shape (A, B), bearing a small process. At 7 and 21 dpi, the majority of cells had a migratory neuroblast morphology, bearing one well-developed leading process, or the morphology of a differentiated granule neuron with an apical dendrite and various short dendrites, or that of a periglomerular neuron (C-F). G, Quantification of the total number of labeled cells at 2, 7, and 21 dpi ($***P = .0001$, one-way analysis of variance [ANOVA] with Tukey's post hoc test). H, At 2 dpi, all the cells were located in the OB core (49.5%) and the iGCL (50.5%). At 7 dpi, the majority of cells were found in the OB core (36.8%) and iGCL (34.2%, $*P = .034$, one-way ANOVA followed by Tukey's post hoc test; 7 vs 2 dpi), although 25.8% cells were detected in the oGCL and a small percentage of EGFP-labeled cells were in the ML and PL (2.4%), or the GL (0.8%). At 21 dpi, a small percentage of cells (2.8%) remained in the OB core ($***P = .0001$ vs 2 dpi, one-way ANOVA followed by Tukey's post hoc test; $###P = .0001$ vs 7 dpi, one-way ANOVA followed by Tukey's post hoc test). At 21 dpi, 23.7% of cells were in the iGCL ($**P = .0034$, one-way ANOVA followed by Tukey's post-test; 21 dpi vs 2 dpi). However, most of the cells had migrated to the oGCL (44.9%; $**P = .0023$, unpaired *t* test, two-tailed, *df* = 4, *t* = 6.946; 21 dpi vs 7 dpi), the ML and PL (9%), or the GL (16.9%; E, F, H). Bars represent the mean \pm SEM (*n* = 3 animals per time point). Scale bar (shown in F) = 72.1 μ m (A, C, E); 64.1 μ m (B, D, F); PLs, plexiform layers (internal and external). I-N, An EGFP-expressing retroviral vector was injected into the adult OB core to label progenitor cells and assess their morphology at 1 to 3 dpi after immunostaining with an antibody against GFP. The cells were assigned as Stellate (I), Globular (J), Branched (K), and Migratory (L), based on their morphology. M, Branched cells were significantly more abundant than stellate cells at 1 dpi ($**P = .0079$; one-way ANOVA with Tukey's post hoc test). N, At 1 dpi, the cycling (MCM2⁺) and the EGFP⁺ population was composed of globular, branched, and migratory cells, whereas stellate cells were also observed at 2 and 3 dpi. At 3 dpi, there was a significant reduction in the percentage of MCM2⁺ migratory cells ($*P = .0395$, 3 vs 1 dpi; unpaired Student's *t* test, *t* = 2.406, *df* = 9), possibly because they had migrated out of the OB core toward the iGCL. The proportion of MCM2⁺ globular cells in the OB core was almost constant over the 3-day period (37.1%-41.6%). Scale bar (shown in F and L) = 30.8 μ m. GL, glomerular layer; iGCL, inner granule cell layer; ML, mitral layer; NSCs, neural stem cells; OB, olfactory bulb; oGCL, outer granule cell layer

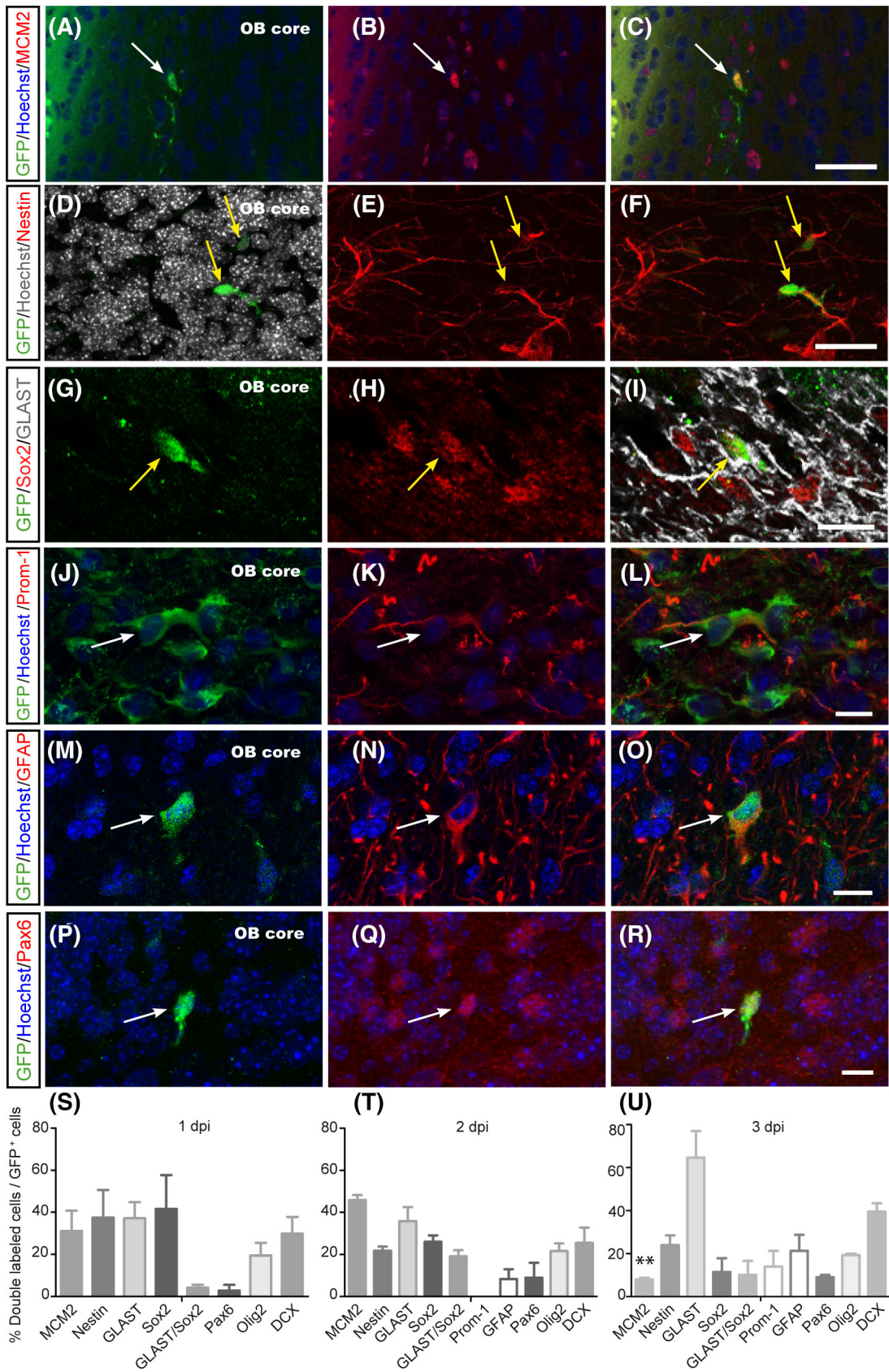


FIGURE 4 Legend on next page.

globular cells with a round or globular cell body without visible processes; branched, polygonal-like cells with one to two thin processes; and migratory cells with an elongated cell body, and a leading and a trailing process, taking a previous study⁴ as a reference for this analysis. Among these cell types, the branched cells were significantly more abundant than the stellate cells at 1 dpi (** $P = .0079$; one-way ANOVA with Tukey's post hoc test), although these differences were not significant at 2 dpi (Figure 3M).

We then sought to determine the proportion of labeled cells that were proliferating at these early time points. At 1 dpi, the EGFP⁺ population of cycling cells (MCM2⁺) was composed of globular, branched, and migratory cells (Figure 3N), whereas at 2 and 3 dpi cycling stellate cells were also observed. At 3 dpi, a change in the cell composition was evident, with a significant reduction in the proportion of MCM2⁺ migratory cells (* $P = .0395$, 3 vs 1 dpi; unpaired two-tailed Student's *t* test, $t = 2.406$, $df = 9$). By contrast, the proportion of MCM2⁺ stellate cells increased from day 2 to 3 dpi. Finally, the proportion of MCM2⁺ globular cells in the OB core remained virtually constant over the 3-day period (37.1%-41.6%; Figure 3N). Hence, the OB core appears to contain a variety of cells with morphologies that resemble those of NSCs and of migratory neuroblasts.

3.3.3 | Adult OB core progenitor cells express molecular markers of NSCs, committed progenitors, and neuroblasts

We analyzed the expression of molecular markers by the cells in the OB core at early time points (Figures 4 and S2) in order to distinguish between cycling cells (MCM2⁺), putative aNSCs (expressing Nestin, GLAST/Slc1a3, Sox2, Prominin-1/CD133, and GFAP),^{4,6,7,16,28,29,38,42,45-56} progenitor cells committed to the neuronal lineage (Pax6)^{57,58} or to the oligodendroglial lineage (Olig2),⁵⁹ neuroblasts and immature neurons (DCX).⁶⁰ Although a single marker is not exclusively expressed by NSCs, the combination of Nestin, GLAST, Sox2, Prominin-1, and GFAP is widely used to identify NSCs in the adult brain (see references above). For simplicity, images of dual

and triple staining for these markers are shown at 2 dpi, except for Prominin-1 which is shown at 3 dpi (Figures 4A-R and Figure S2), whereas the quantitative analyses are presented at 1, 2, and 3 dpi (Figure 4S-U). As expected, MCM2, Sox2, Pax6, and Olig2 staining was nuclear (Figures 4B,H,Q and S2B), the Nestin antibody labeled intermediate filaments (Figure 4E), GLAST labeling was restricted to the membrane (Figure 4I), Prominin-1⁶¹ and GFAP antibodies immunostained the cell body and processes (Figure 4K,N), and DCX was abundantly expressed in neurites and in the contours of the cell bodies (Figure S2E). The quantitative analysis (Figure 4S-U) indicated that cycling (MCM2⁺) cells were relatively abundant at 1 and 2 dpi (35%-46% of the total EGFP⁺ cell population), yet there was a significant decrease in these cells at 3 dpi (** $P = .0039$, one-way ANOVA with Tukey's post hoc test; 3 dpi vs 2 dpi). Cells expressing Nestin and Sox2 were also abundant at 1 dpi (37.5%-41.7%), and while there appeared to be a reduction in the number of these cells at 2 and 3 dpi, this was not a significant change. Cells expressing both GLAST and Sox2, a marker combination characteristic of NSCs,²⁹ represented 4.2% to 19.2% of the EGFP⁺ cells, whereas the GLAST⁺ cell percentage appeared to increase from 2 to 3 dpi although this increase was not significant. Prominin-1 was not detected at 2 dpi ($n = 3$ mice), although it was expressed in 14% of the EGFP⁺ cells at 3 dpi. By contrast, GFAP was detected in 8.4% and 21.3% of the EGFP⁺ cells located in the OB core at 2 dpi and 3 dpi, respectively. EGFP⁺ cells expressing GFAP were very rare at 1 dpi ($n = 3$). Although GFP⁺NeuN⁻ cells preferentially formed small clusters of globular cells at the edge of the OB core (Figure 2F,G), the Nestin⁺, GLAST⁺Sox2⁺, Prominin-1⁺, and GFAP⁺ cells were found throughout the OB core. Nonetheless, the spatial organization of the NSCs in the OB core will require further study.

The percentages of Pax6⁺ and DCX⁺ cells varied between 2.7% and 9.0% and 29.9% and 39.6%, respectively, although these did not represent statistically significant variations between days 1 to 3 dpi. In addition, there was a relatively constant proportion of Olig2⁺ cells (19.3%-21.7%) over this period. Together, these results indicate that the adult OB core contains cells that express molecular markers typical of aNSCs, committed progenitors to the neuronal or the oligodendroglial lineage and neuroblasts.

FIGURE 4 Molecular markers expressed by enhanced green fluorescent protein (EGFP)-labeled cells in the adult OB core indicate the existence of NSCs, committed progenitors and neuroblasts. An EGFP-expressing retroviral vector was injected into the OB core of 9-week-old mice. Animals were anesthetized and perfused at 1, 2, and 3 days postinjection (dpi), and then, immunohistochemistry using specific antibodies was performed in order to label GFP and cycling cells (MCM2, A-C), or putative NSCs (Nestin, D-F; Sox2/GLAST, G-I; Prominin-1/Prom-1, J-L; glial fibrillary acidic protein [GFAP], M-O) or committed progenitor cells to the neuronal lineage (Pax6, P-R), and to the oligodendroglial lineage (Olig2, see Figure S2) and neuroblasts (DCX, see Figure S2). Sections were counterstained with Hoechst (not shown in D-I). For simplicity, images are shown at 2 dpi (Prominin-1 is shown at 3 dpi), whereas data from the quantitative analyses performed at 1, 2, and 3 dpi are presented (S-U). MCM2⁺ cells were relatively abundant at 1 and 2 dpi (35%-46% of the total EGFP⁺ cell population) with a significant decrease at 3 dpi (** $P = .0039$, one-way analysis of variance [ANOVA] with Tukey's post hoc test; 3 vs 2 dpi). Cells expressing Nestin and Sox2 were also abundant at 1 dpi (37.5%-41.7%) and underwent nonsignificant reductions at 2 and 3 dpi. Cells expressing both GLAST and Sox2, a marker combination characteristic of olfactory bulb NSCs, represented 4.2% to 19.2% of the EGFP⁺ cells. Prominin-1 was detected in 14% of EGFP⁺ cells at 3 dpi, and GFAP in 8.4% and 21.3% of EGFP⁺ cells at 2 dpi and 3 dpi, respectively. The percentage of Pax6⁺ cells and of DCX⁺ cells varied between 2.7% and 9.0% and 29.9% and 39.6%, respectively, whereas a relatively constant proportion of Olig2⁺ cells (19.3%-21.7%) was detected. Bars represent the mean \pm SEM ($n = 3$ animals per time point). Scale bars = 24.6 μ m (A-F), 15 μ m (G-I), 10 μ m (J-R). DCX, doublecortin; NSCs, neural stem cells; OB, olfactory bulb

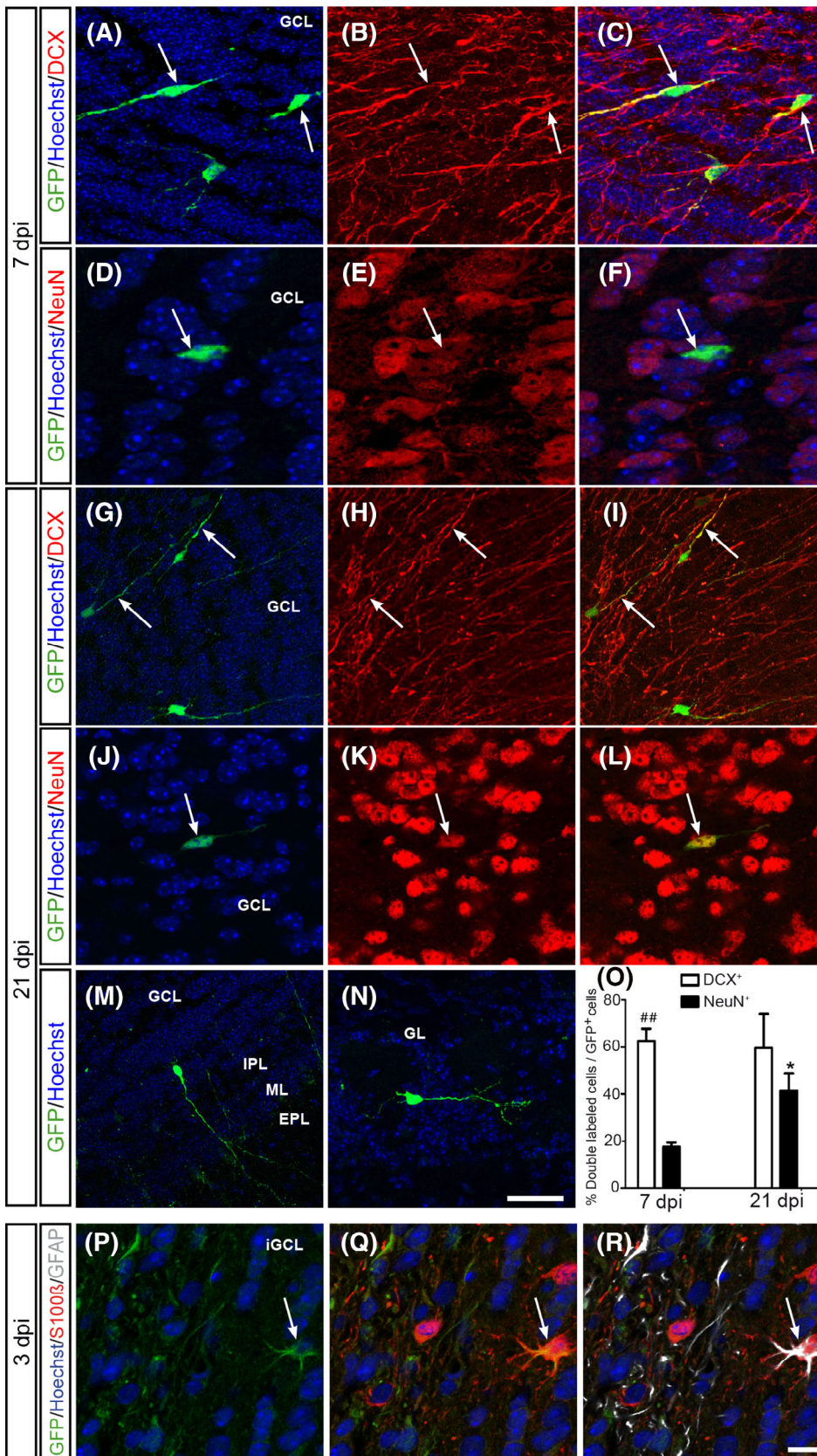
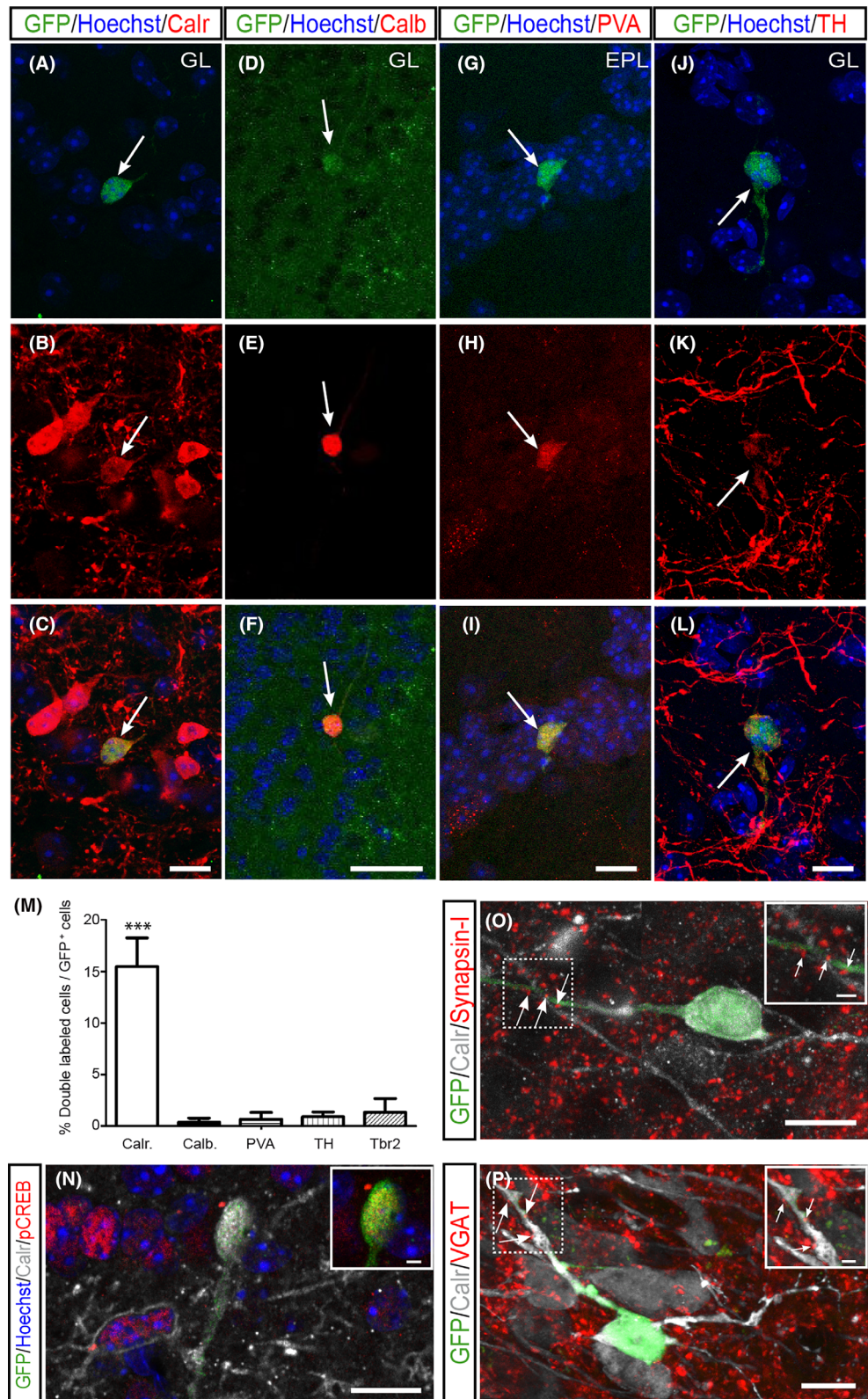


FIGURE 5 Molecular markers expressed by newly generated neurons and astrocytes from adult OB core NSCs. An enhanced green fluorescent protein (EGFP)-expressing retroviral vector was injected into the OB core of 9-week-old mice in order to label the progeny of proliferative cells using dual (GFP/Marker) or single (GFP) immunohistochemistry on vibratome sections at 7 and 21 days postinjection (dpi). Sections were counterstained with Hoechst. EGFP⁺DCX⁺ neuroblasts/immature neurons (A-C, G-I) and EGFP⁺NeuN⁺ neurons (D-F, J-L) were detected at both time points. M,N, Newly generated neurons acquired highly elaborate morphologies in the GCL and GL at 21 dpi. O, At 7 dpi, EGFP⁺DCX⁺ cells were more abundant than EGFP⁺NeuN⁺ cells ($^{##}P = .0013$, unpaired two-tailed Student's *t* test; $t = 8.061$, $df = 4$), while the percentage of EGFP⁺ cells expressing DCX remained relatively constant (59.7%) between 7 and 21 dpi. By contrast, there was a significant 2.3-fold increase in the percentage of EGFP⁺ cells expressing NeuN cells between 7 (17.6%) and 21 dpi (41.4%; $^*P = .0284$; unpaired two-tailed Student's *t* test, $t = 3.978$, $df = 3$). P-R, The images show a newly generated astrocyte coexpressing S100 β and glial fibrillary acidic protein (GFAP) at 3 dpi. Bars represent the mean \pm SEM ($n = 3$ animals per time point). Scale bars (shown in N and R) = 13.45 μ m (A-F), 42.4 μ m (G-I), 22.4 μ m (J-L), 50.6 μ m (M, N), 10 μ m (P-R). GCL, granule cell layer; GL, glomerular layer; NSCs, neural stem cells; OB, olfactory bulb

FIGURE 6 Adult OB core NSCs predominantly generate Calr⁺-interneurons with a high degree of maturation. An enhanced green fluorescent protein (EGFP)-expressing retroviral vector was injected into the OB core of 9-week-old mice to study the neuron progeny of proliferative cells and its maturation at 21 to 22 days postinjection (dpi) by dual and triple immunohistochemistry on vibratome sections with antibodies against GFP and Calr, Calb, PVA, TH, Tbr2, pCREB, Synapsin-I, or VGAT. Sections were counterstained with Hoechst (not shown for clarity in some panels). We found EGFP⁺ Calr⁺ cells in all layers of the OB (A-C, a double labeled cell is shown in the GL), EGFP⁺ Calb⁺ cells in the GL (D-F), EGFP⁺ PVA⁺ cells in the EPL (G-I), EGFP⁺ TH⁺ cells in the GL (J-L), and EGFP⁺ Tbr2⁺ cells in the GL (shown in Figure S4). M, The graph shows the percentage of double positive cells, of which Calr⁺ cells were the most abundant (15.5%) neuron population generated from the OB core NSCs, whereas the percentages of Calb⁺, PVA⁺, TH⁺, and Tbr2⁺ cells were 11 to 40 times lower ($***P < .0001$ for Calr vs Calb, Calr vs PVA, Calr vs TH, and Calr vs Tbr2; analysis of variance [ANOVA] followed by Tukey's post hoc test). Bars represent the mean \pm SEM ($n = 3$ animals per cell marker). O,P, Newly generated Calr⁺ neurons express pCREB at 22 dpi, as well as the presynaptic proteins Synapsin-I and VGAT, which concentrate in boutons (better visualized in the higher magnification insets). Scale bars = 10 μ m (A-C, G-L, N-P, insets 2 μ m); 16.5 μ m (D-F). EPL, external plexiform layer; GL, glomerular layer; NSCs, neural stem cells; OB, olfactory bulb



3.3.4 | Adult OB core NSCs generate mature interneuron subtypes in vivo

To study the neuronal differentiation of the EGFP⁺ cells, sections were immunostained for DCX and for the mature neuronal marker

NeuN^{30,62,63} at 7 and 21 dpi (Figure 5). We found EGFP⁺ DCX⁺ neuroblasts/immature neurons (Figure 5A-C,G-I) and EGFP⁺ NeuN⁺ mature neurons (Figure 5D-F,J-L) at both time points. At 7 dpi, the EGFP⁺ DCX⁺ cells were more abundant than the EGFP⁺ NeuN⁺ cells ($***P = .0013$, unpaired two-tailed Student's *t* test, $t = 8.061$, $df = 4$:

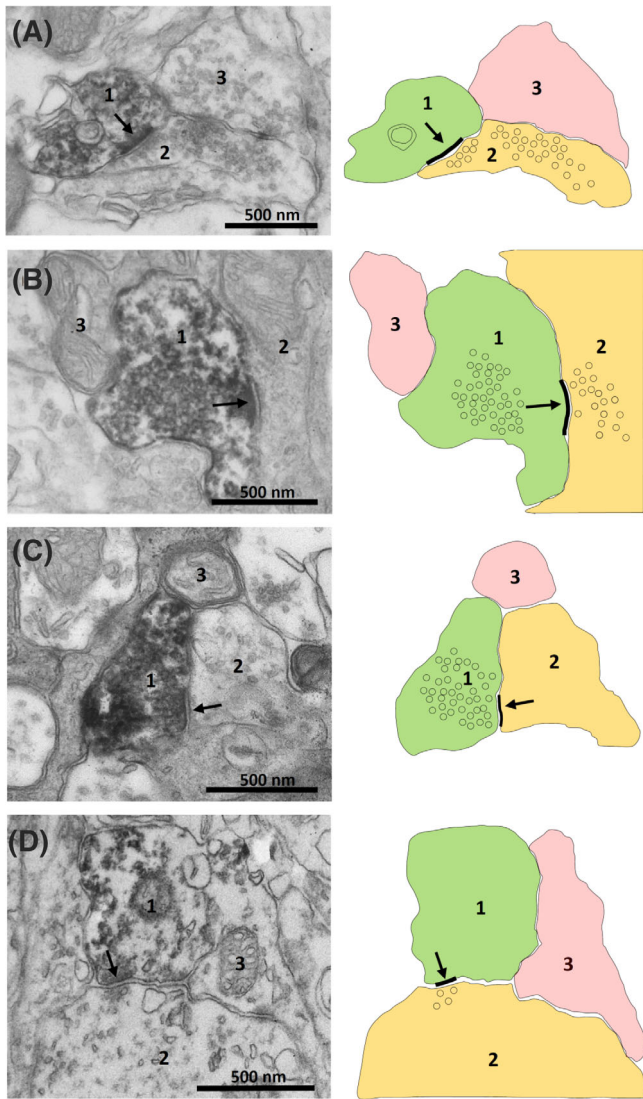


FIGURE 7 Newly generated neurons from the adult OB core NSCs establish synapses in vivo. An enhanced green fluorescent protein (EGFP)-expressing retroviral vector was injected into the OB core of 9-week-old mice to visualize the synapses established by newly generated neurons at 28 dpi. After enhanced green fluorescent protein-3,3'-diaminobenzidine (EGFP-DAB) immunostaining, the synaptic relationships of the newly generated neurons were analyzed by electron microscopy. Synaptic contacts are indicated by arrows located on the postsynaptic element. The drawings on the right represent the profiles shown in the electron micrographs. In all panels, EGFP-DAB immunostained profiles are indicated by the number 1 and in green; profiles that establish synaptic relationships with those that contain EGFP-DAB precipitate are indicated by the number 2 and are in the orange domain; and unlabeled profiles are indicated by the number 3 and they are in the pink region. A, A dendrite containing DAB receives an asymmetric synapse from an axon-like process. The dendrite belongs to the small PGC indicated by an open arrow in the resin block shown in Figure S5. B, A dendrite containing DAB receives an asymmetrical synaptic contact from the olfactory nerve. The dendrite belongs to the large PGC indicated by a solid arrow in the resin block shown in Figure S5. C, A DAB-containing process establishes a symmetrical synapse on an unlabeled profile in the GL. D, The dendrite of a granule cell containing DAB receives an asymmetric synapse from the dendrite of a mitral or tufted cell in the EPL. Scale bars = 500 nm. EPL, external plexiform layer; GL, glomerular layer; NSCs, neural stem cells; OB, olfactory bulb; PGC, periglomerular cell

Figure 5O) and the proportion of EGFP⁺ cells expressing DCX remained relatively constant at both time points. By contrast, there was a significant 2.3-fold increase in the proportion of EGFP⁺ cells expressing NeuN between 7 dpi (17.6%) and 21 dpi (41.4%: **P* = .0284; unpaired two-tailed Student's *t* test, *t* = 3.978, *df* = 3: Figure 5O), indicating that these neurons mature. The differentiation/maturation of newly generated neurons was further confirmed by the presence of EGFP⁺ neurons with elaborate morphologies in the GCL and GL at 21 dpi (Figure 5M,N). Hence, the large majority of EGFP⁺-derived cells at 21 dpi belong to the neuronal lineage (Figure 5O). Next, we used the coexpression of both S100 β and GFAP in EGFP⁺ cells as a criterion to identify astrocyte generation from OB-NSCs, and we found a small number of EGFP⁺S100 β ⁺GFAP⁺ cells in the GCL (Figure 5P-R). This colabeling was important as GFAP is also expressed by aNSCs (see above) and S100 β is detected in a subpopulation of OB oligodendrocytes.⁶⁴ EGFP⁺ cells expressing S100 β but not GFAP were also found (Figure S3). In summary, when compared to SVZ-NSCs, OB-NSCs appear to have a similar output in terms of the generation of neural lineages in normal adulthood.

We then investigated what type of neurons might be generated by the OB core RV-EGFP-labeled cells at 21 dpi (Figure 6). To examine the subpopulations of major OB interneuron subtypes, we performed dual immunostaining for GFP along with the calcium binding proteins Calr, Calb, or PVA, as well as for the dopaminergic neuron marker tyrosine hydroxylase (TH).^{16,21,22,65,66} We also examined whether glutamatergic juxtglomerular neurons (Tbr2)^{14,67} could be generated from OB-NSCs. We found double labeled EGFP⁺Calr⁺ cells in the GL and GCL (Figure 6A-C), EGFP⁺Calb⁺ cells in the GL (Figure 6D-F), EGFP⁺PVA⁺ cells in the EPL (Figure 6G-I), and EGFP⁺TH⁺ and EGFP⁺Tbr2⁺ cells in the GL (Figures 6J-L and S4A-C). Of the neurons studied here, Calr⁺ cells were the most abundant cell type generated from OB core NSCs (15.5% of the total GFP⁺ cells: Figure 6M), with the percentages of Calb⁺, PVA⁺, TH⁺, and Tbr2⁺ cells some 11 to 40 times lower than that of the Calr⁺ cells (***P* < .0001 for Calr vs Calb, Calr vs PVA, Calr vs TH, and Calr vs Tbr2; ANOVA followed by Tukey's post hoc test: Figure 6M). This is consistent with the greater abundance of Calr⁺ neurons in the OB compared to that of other interneuron subtypes.^{9,22} Collectively, our results show that there are NSCs in the OB core that mainly differentiate into Calr⁺-interneurons, with other granule and periglomerular cells (PGCs) generated more sparsely. To our knowledge, this is the first time this type of analysis has been performed on locally generated OB neurons,^{23,25,26,28} although it has been carried out on the neuronal progeny that originates in the SVZ and RMS, and that subsequently incorporates into the OB.^{7,9,10,12,14,17,40,41,43,68,69} To explore the degree of maturation of the newly formed Calr⁺ neurons, vibratome sections were triple-immunostained with antibodies against GFP and Calretinin in combination with an antibody against the transcription factor pCREB,^{70,71} or with antibodies against the presynaptic markers synapsin-I and vesicular GABA transporter (VGAT).⁷² Nearly all EGFP⁺Calr⁺ cells expressed pCREB (such as the cell depicted in Figures 6N and S4D,E), while we also found EGFP⁺Calr⁺ cells immunolabeled with synapsin-I and with VGAT (Figures 6O,P and S4F-I).

Moreover, synapsin-I and VGAT immunolabeling accumulated in boutons, which were located either on neurons making synapses with the EGFP⁺Calr⁺ cells (red boutons) or within these EGFP⁺Calr⁺ cells (orange boutons).

3.3.5 | Newly generated neurons from adult OB core NSCs make and receive synaptic contacts in vivo

To confirm the synaptic maturation of the newly generated neurons, it was fundamental to analyze whether or not they established structural synapses with OB circuits in vivo (Figure 7). After EGFP-DAB staining of vibratome sections, we confirmed the presence of labeled granule cells and PGCs (not shown). A resin block that contained two PGCs was re-embedded for transmission electron microscopy (TEM) processing⁷³ (Figure S5A), identifying synaptic contacts (arrows) and EGFP⁺ cells (containing a black precipitate; green in the cartoons) in the images obtained (Figures 7A-D and S5B,C). Newly generated PGCs received synaptic contacts, as the small PGC studied (Figure S5A, open arrow) clearly received an asymmetric synapse from an axon-like process (Figure 7A). In addition, part of the large PGC (Figure S5A, solid arrow) received an asymmetric synapse from the olfactory nerve (Figure 7B). The electron dense region of the nerve at the synapse indicates that this is the presynaptic terminal and that the PGC has a discernible postsynaptic density. Symmetrical synaptic contacts were evident where the presynaptic EGFP-labeled cells containing vesicles connected the nonlabeled postsynaptic cell (Figure 7C). Finally, the dendrite in the EPL of a granule cell received an asymmetric synapse from the dendrite of a mitral or tufted cell (Figure 7D). In conclusion, all these findings demonstrate for the first time that neurons generated from adult OB core NSCs establish asymmetric and symmetric synaptic contacts.

4 | DISCUSSION

The V-SVZ of the lateral ventricle and the SGZ in the hippocampal dentate gyrus are well-characterized neurogenic niches in the postnatal and adult mouse brain, and the NSCs in these structures produce a variety of neurons through intermediate dividing progenitors.⁷ The presence of NSCs and neurogenesis is also thought to occur in other brain regions, such as the hypothalamus and the OB.^{23,27-29,74} However, since the OB also receives neurons that originate in the V-SVZ^{2,4,7} and from the RMS elbow,^{42,43} it remains unclear whether neurogenesis in the adult OB occurs through local resident progenitor cells or not. Here, stereotaxic injections of retroviral and LV particles (expressing EGFP) into the mouse OB core and the SVZ, in conjunction with morphological analysis and cell-type specific immunolabeling, provides evidence that a population of neurogenic and gliogenic NSCs do reside in the adult OB core. These cells give rise to Calr⁺-neurons, whereas other OB neuron subtypes are generated more sparingly. Crucially, the newly generated neurons establish and receive synapses with and from host neurons, they develop

neurotransmission machinery and they possibly respond to synapse activation by triggering CREB phosphorylation, suggesting they incorporate into the OB's circuits.

4.1 | Progenitor cells located in the adult mouse OB core possess features of NSCs, and of committed neuronal and glial progenitors

After injecting a retroviral vector into the core of the OB in vivo, we detect four main cell morphologies that are similar to those found previously in a pioneering study of the adult mouse SVZ.⁴ Specifically, stellate cells in the SVZ are type B NSCs that express GFAP and that generate neurons via an intermediate globular cell type. Here, cells with a stellate morphology are detected as early as 1 dpi, although as dividing MCM2⁺ cells with a stellate morphology are only found at 2 and 3 dpi, these OB stellate cells may divide slowly. The existence of slowly dividing NSCs in the adult OB was reported previously^{23,29} and indeed, we identified LRCs in the OB core.

Our detailed labeling technique and analysis reveals a constant proportion of dividing (MCM2⁺) globular cells during the first three dpi, which might correspond to intermediate progenitors.⁴ By contrast, the proportion of MCM2⁺-migratory cells drops from day 1 to 3 pi, indicating that this cell population may exit the cell cycle to differentiate into neurons. Concurring with our morphological analysis, immunohistochemistry shows that the OB core contains a variety of cell types, including: NSCs, progenitors restricted to the neuronal lineage as well as neuroblasts. The fact that EGFP⁺ cells expressing Prominin-1 or GFAP were either not detected or very rare at 1 dpi relative to those expressing Nestin perhaps suggests that the former correspond to NSCs in a less active state than the Nestin⁺ NSCs. Together, our results support the existence of NSCs and intermediate progenitors in the OB core, which mainly produce neurons but also astrocytes to a lesser extent. Moreover, the presence of a nearly constant population of EGFP-labeled Olig2⁺ cells at 1 to 3 dpi suggests that the OB core may be a source of oligodendrocytes.

4.2 | Adult OB core NSCs give rise to Calretinin⁺ and other neuronal subtypes capable of establishing synapses in vivo

There are at least 10 subtypes of interneurons generated from SVZ NSCs, as detected using a combination of cell markers and morphological analyses.^{9,10,69,75,76} Using a cell marker approach, we detected four different interneuron populations that originate from the OB core NSCs and that migrate to different OB layers, mainly the GCL (Calr⁺), the GL (Calr⁺, Calb⁺, TH⁺), and the EPL (PVA⁺). In addition to GABAergic interneurons, we observed glutamatergic juxtglomerular neurons in the GL (Tbr2⁺). Of the populations studied here, the Calr⁺-cells were by far the most abundant, suggesting that OB core NSCs are predetermined to produce mostly Calr⁺-interneurons. By contrast, NSCs located in the RMS elbow appear to be specified to give rise to

dopaminergic neurons although granule cells are also generated in this region.⁴⁰⁻⁴⁴ Together these previous findings and ours argue against the possibility that the viral particles infect cells in the RMS elbow after our injections. Therefore, our results support and extend the concept that NSCs residing in defined microdomains within the V-SVZ, RMS elbow and OB core are largely predetermined to produce specific interneuron types.

The EM analysis shows that neurons generated from the OB core-NSCs develop dendritic spines and synaptic vesicles, allowing them to establish both symmetric and asymmetric synaptic contacts with OB neurons and the olfactory nerve. Specifically, neurons generated from OB-NSCs that are located in the GL receive synapses from the olfactory nerve and they establish dendro-dendritic synaptic contacts with mitral/tufted cells, synapses frequently observed in the OB.⁷³ Moreover, granule neurons derived from OB-NSCs establish dendro-dendritic synapses with mitral/tufted cells in the EPL, as do granule cells. The synaptic pattern of these neurons appears to be similar to that described for SVZ-generated interneurons that migrate through the RMS and establish connections in the OB.⁷⁷ Thus, our findings suggest that OB core-generated periglomerular neurons may receive sensory input in the glomerular neuropil. Furthermore, the dendro-dendritic synaptic contacts of OB core-generated granule neurons with mitral and tufted cells suggest that the new neurons may be functionally integrated into the bulbar circuits. Indeed, the presence of phosphorylated CREB in Calr⁺ cells indicates these neurons can respond to synaptic activation.

The mammalian OB is a very plastic structure that plays a fundamental role in the transmission of olfactory information in rodents and humans. Although OB plasticity in mice largely relies on adult neurogenesis, this remains unclear in humans. On the one hand, NSCs have been isolated from human OB tissue,^{27,34-37} and cells expressing immature neuronal markers, proliferative markers, and Nestin have been identified in the GCL and core of postmortem human OB samples,^{24,27} supporting the existence of neurogenesis in the adult human OB. On the other hand, cytoarchitectural studies tracking the development of the human SVZ and RMS over the first months and years of life,⁷⁸ as well as studies measuring the age of human OB neurons using ¹⁴C dating,⁷⁹ suggest that adult human OB neurogenesis is very limited or even nonexistent. Interestingly, volumetric measurements of the human OB show changes in volume that correlate with olfactory function in normosmic subjects and in patients suffering from pathologies associated with anosmia.⁸⁰ We cannot currently establish the cellular mechanisms underlying such OB plasticity, which may or may not be linked to neurogenesis, or to other plastic processes like synaptogenesis at the level of the glomerulus.

Sensory deprivation decreases OB volume, not only in humans but also in animal models, and it has also been shown that neurogenesis in the adult murine OB is very sensitive to sensory experience.^{81,82} In this regard, follow-up studies in patients suffering from anosmia may provide insight into the cellular mechanisms underlying OB plasticity. Recently, olfactory dysfunction has been associated

with the course of COVID-19 disease, probably due to the viral infection of ACE2-expressing sustentacular cells in the olfactory epithelium.^{83,84} In turn, this is likely to negatively affect the adjacent olfactory sensory neurons that transduce the olfactory information to second-order neurons in the OB. A recent study provided evidence of the presence of the virus in postmortem OB tissue from three COVID-19 patients,⁸⁵ yet more studies are needed to fully interpret these data.^{84,86}

Thus, we can conclude that despite the fact neurogenesis has not been detected in the human OB in all the studies performed to date, it cannot be ruled out that OB neurogenesis could take place under specific circumstances and perhaps, become reactivated through local NSCs. Indeed, brain injuries activate cell proliferation in the SVZ and increase the migration of neuroblasts to injured areas, deviating them from their normal route.⁸⁷ Determining whether local cells in the human OB with NSC potential can be stimulated under pathological and physiological conditions, and even produce new functional interneurons, could be a key area of study in the near future.

5 | CONCLUSION

In this study, we present new evidence that NSCs exist within the core of the adult mouse OB and that they predominantly produce Calr⁺ interneurons. Our findings also demonstrate for the first time that these newly generated neurons incorporate into the adult OB synaptic circuits by establishing active synapses with existing neurons and the olfactory nerve. Understanding whether this process is conserved in other mammalian species, including humans, warrants further investigation.

ACKNOWLEDGMENTS

We thank M^ª José Román (Instituto Cajal-CSIC, Madrid, Spain) for her technical support, Dr Mark Sefton (BiomedRed, Madrid, Spain) for English editing, and Paula Vicario and Lucía Vicario (Instituto Cajal-CSIC, Madrid, Spain) for helping with the image analysis. This work was funded by grants from the Spanish “Ministerio de Economía y Competitividad and Ministerio de Ciencia, Innovación y Universidades” (MINECO and MICIU: SAF2013-4759R and SAF2016-80419-R, PID2019-109059RB-I00 to C.V., SAF2015-70433-R to H.M., BFU2016-80870-P to A.C., and CIBERNED CB06/05/0065 to C.V.), from the “Comunidad de Madrid” (S2011/BMD-2336) to C.V. and H.M., from the “Generalitat Valenciana” (PROMETEO/2018/055) to H.M., and from the CSIC Intramural program (Refs. 201220E098 and 201320E054) to C.V. Additional support was provided by the European Research Council (ERC) 2012-StG (311736-PD-HUMMODEL), the Instituto de Salud Carlos III - ISCIII/FEDER (Red de Terapia Celular - TerCel RD16/0011/0024 and PIE14/00061) to A.C. Ç.D. received a short-term fellowship from the Red Olfativa Española (ROE). M.M.-E, M.D.-M., A.H.-C., and V.N.-E. were supported by FPI Fellowships from the MICINN and MINECO.

CONFLICT OF INTEREST

The authors declared no potential conflicts of interest.

AUTHOR CONTRIBUTIONS

C.D.: design, collection and assembly of data, data analysis and interpretation, manuscript writing; M.M.-E., C.C.: design, collection and assembly of data, data analysis and interpretation; E.D.-G.: collection and assembly of data, data analysis and interpretation; M.D.-M., E.V.-V., V.N.-E., A.H.-C.: collection and assembly of data; A.C.: design, provision of study material, financial support; H.M.: conception and design, data analysis and interpretation, financial and administrative support, manuscript writing; C.V.: conception and design, collection and assembly of data, data analysis and interpretation, financial and administrative support, manuscript writing and final approval of manuscript.

DATA AVAILABILITY STATEMENT

The data that support the findings of this study are available on request from the corresponding author.

ORCID

Carlos Vicario  <https://orcid.org/0000-0002-7060-0250>

REFERENCES

- Mizrahi A. Dendritic development and plasticity of adult-born neurons in the mouse olfactory bulb. *Nat Neurosci*. 2007;10(4):444-452.
- Ponti G, Obernier K, Guinto C, Jose L, Bonfanti L, Alvarez-Buylla A. Cell cycle and lineage progression of neural progenitors in the ventricular-subventricular zones of adult mice. *Proc Natl Acad Sci USA*. 2013;110(11):E1045-E1054.
- Adams KV, Morshead CM. Neural stem cell heterogeneity in the mammalian forebrain. *Prog Neurobiol*. 2018;170:2-36.
- Doetsch F, Caille I, Lim DA, et al. Subventricular zone astrocytes are neural stem cells in the adult mammalian brain. *Cell*. 1999;97(6):703-716.
- Lois C, Álvarez-Buylla A. Long-distance neuronal migration in the adult mammalian brain. *Science*. 1994;264(5162):1145-1148.
- Codega P, Silva-Vargas V, Paul A, et al. Prospective identification and purification of quiescent adult neural stem cells from their in vivo niche. *Neuron*. 2014;82(3):545-559.
- Obernier K, Alvarez-Buylla A. Neural stem cells: origin, heterogeneity and regulation in the adult mammalian brain. *Development*. 2019;146(4):1-15.
- Basak O, Taylor V. Stem cells of the adult mammalian brain and their niche. *Cell Mol Life Sci*. 2009;66(6):1057-1072.
- Merkle FT, Fuentealba LC, Sanders TA, Magno L, Kessaris N, Alvarez-Buylla A. Adult neural stem cells in distinct microdomains generate previously unknown interneuron types. *Nat Neurosci*. 2014;17(2):207-214.
- Wen Y, Zhang Z, Li Z, et al. The PROK2/PROKR2 signaling pathway is required for the migration of most olfactory bulb interneurons. *J Comp Neurol*. 2019;527:2931-2947.
- Ravi N, Sanchez-Guardado L, Lois C, Kelsch W. Determination of the connectivity of newborn neurons in mammalian olfactory circuits. *Cell Mol Life Sci*. 2017;74(5):849-867.
- Lledo PM, Merkle FT, Alvarez-Buylla A. Origin and function of olfactory bulb interneuron diversity. *Trends Neurosci*. 2008;31(8):392-400.
- Mobley AS, Bryant AK, Richard MB, Brann JH, Firestein SJ, Greer CA. Age-dependent regional changes in the rostral migratory stream. *Neurobiol Aging*. 2013;34(7):1873-1881.
- Brill MS, Ninkovic J, Winpenny E, et al. Adult generation of glutamatergic olfactory bulb interneurons. *Nat Neurosci*. 2009;12(12):1524-1533.
- Fiorelli R, Azim K, Fischer B, Raineteau O. Adding a spatial dimension to postnatal ventricular-subventricular zone neurogenesis. *Development*. 2015;142(12):2109-2120.
- Curto GG, Nieto-Estevez V, Hurtado-Chong A, et al. Pax6 is essential for the maintenance and multi-lineage differentiation of neural stem cells, and for neuronal incorporation into the adult olfactory bulb. *Stem Cells Dev*. 2014;23(23):2813-2830.
- Bonzano S, Bovetti S, Gendusa C, et al. Adult born olfactory bulb dopaminergic interneurons: molecular determinants and experience-dependent plasticity. *Front Neurosci*. 2016;10:189.
- Fujiwara N, Cave JW. Partial conservation between mice and humans in olfactory bulb interneuron transcription factor codes. *Front Neurosci*. 2016;10:337.
- Moreno N, Morona R, Lopez JM, et al. Anuran olfactory bulb organization: embryology, neurochemistry and hodology. *Brain Res Bull*. 2008;75(2-4):241-245.
- Kosaka K, Kosaka T. Chemical properties of type 1 and type 2 periglomerular cells in the mouse olfactory bulb are different from those in the rat olfactory bulb. *Brain Res*. 2007;1167:42-55.
- Parrish-Aungst S, Shipley MT, Erdelyi F, Szabo G, Puche AC. Quantitative analysis of neuronal diversity in the mouse olfactory bulb. *J Comp Neurol*. 2007;501(6):825-836.
- Hurtado-Chong A, Yusta-Boyo MJ, Vergaño-Vera E, Bulfone A, de Pablo F, Vicario-Abejón C. IGF-I promotes neuronal migration and positioning in the olfactory bulb and the exit of neuroblasts from the subventricular zone. *Eur J Neurosci*. 2009;30(5):742-755.
- Giachino C, Taylor V. Lineage analysis of quiescent regenerative stem cells in the adult brain by genetic labelling reveals spatially restricted neurogenic niches in the olfactory bulb. *Eur J Neurosci*. 2009;30(1):9-24.
- Bedard A, Parent A. Evidence of newly generated neurons in the human olfactory bulb. *Brain Res Dev Brain Res*. 2004;151(1-2):159-168.
- Fukushima N, Yokouchi K, Kawagishi K, Moriizumi T. Differential neurogenesis and gliogenesis by local and migrating neural stem cells in the olfactory bulb. *Neurosci Res*. 2002;44(4):467-473.
- Gritti A, Bonfanti L, Doetsch F, et al. Multipotent neural stem cells reside into the rostral extension and olfactory bulb of adult rodents. *J Neurosci*. 2002;22(2):437-445.
- Liu Z, Martin LJ. Olfactory bulb core is a rich source of neural progenitor and stem cells in adult rodent and human. *J Comp Neurol*. 2003;459(4):368-391.
- Vergaño-Vera E, Méndez-Gómez HR, Hurtado-Chong A, Cigudosa JC, Vicario-Abejón C. Fibroblast growth factor-2 increases the expression of neurogenic genes and promotes the migration and differentiation of neurons derived from transplanted neural stem/progenitor cells. *Neuroscience*. 2009;162(1):39-54.
- Moreno-Estellés M, González-Gómez P, Hortiguera R, et al. Symmetric expansion of neural stem cells from the adult olfactory bulb is driven by astrocytes via WNT7A. *STEM CELLS*. 2012;30(12):2796-2809.
- Defterali C, Verdejo R, Peponi L, et al. Thermally reduced graphene is a permissive material for neurons and astrocytes and de novo neurogenesis in the adult olfactory bulb in vivo. *Biomaterials*. 2016;82:84-93.
- Tang C, Zhu L, Gan W, et al. Distributed features of vimentin-containing neural precursor cells in olfactory bulb of SOD1G93A transgenic mice: a study about resource of endogenous neural stem cells. *Int J Biol Sci*. 2016;12(12):1405-1414.
- Marei HE, Farag A, Althani A, et al. Human olfactory bulb neural stem cells expressing hNGF restore cognitive deficit in Alzheimer's disease rat model. *J Cell Physiol*. 2015;230(1):116-130.
- Marei HE, Shouman Z, Althani A, et al. Differentiation of human olfactory bulb-derived neural stem cells toward oligodendrocyte. *J Cell Physiol*. 2018;233(2):1321-1329.
- Pagano SF, Impagnatiello F, Girelli M, et al. Isolation and characterization of neural stem cells from the adult human olfactory bulb. *STEM CELLS*. 2000;18(4):295-300.
- Marei HE, Ahmed AE, Michetti F, et al. Gene expression profile of adult human olfactory bulb and embryonic neural stem cell suggests

- distinct signaling pathways and epigenetic control. *PLoS One*. 2012;7(4):e33542.
36. Marei HE, Ahmed AE. Transcription factors expressed in embryonic and adult olfactory bulb neural stem cells reveal distinct proliferation, differentiation and epigenetic control. *Genomics*. 2013;101(1):12-19.
 37. Alizadeh R, Hassanzadeh G, Joghataei MT, et al. In vitro differentiation of neural stem cells derived from human olfactory bulb into dopaminergic-like neurons. *Eur J Neurosci*. 2017;45(6):773-784.
 38. Bohlen V, Halbach O. Immunohistological markers for proliferative events, gliogenesis, and neurogenesis within the adult hippocampus. *Cell Tissue Res*. 2011;345(1):1-19.
 39. Nieto-Estévez V, Queslatti-Morales CO, Li L, Pickel J, Morales AV, Vicario-Abejón C. Brain insulin-like growth factor-I directs the transition from stem cells to mature neurons during postnatal/adult hippocampal neurogenesis. *STEM CELLS*. 2016;34(8):2194-2209.
 40. Hack MA, Saghatelian A, de Chevigny A, et al. Neuronal fate determinants of adult olfactory bulb neurogenesis. *Nat Neurosci*. 2005;8(7):865-872.
 41. Merkle FT, Mirzadeh Z, Álvarez-Buylla A. Mosaic organization of neural stem cells in the adult brain. *Science*. 2007;317(5836):381-384.
 42. Alonso M, Ortega-Perez I, Grubb MS, Bourgeois JP, Charneau P, Lledo PM. Turning astrocytes from the rostral migratory stream into neurons: a role for the olfactory sensory organ. *J Neurosci*. 2008;28(43):11089-11102.
 43. Schweyer K, Ruschoff-Steiner C, Arias-Carrion O, et al. Neuronal precursor cells with dopaminergic commitment in the rostral migratory stream of the mouse. *Sci Rep*. 2019;9(1):13359.
 44. Mendoza-Torrealblanca JG, Martínez-Martínez E, Tapia-Rodríguez M, et al. The rostral migratory stream is a neurogenic niche that predominantly engenders periglomerular cells: in vivo evidence in the adult rat brain. *Neurosci Res*. 2008;60(3):289-299.
 45. Llorens-Bobadilla E, Zhao S, Baser A, Saiz-Castro G, Zwadlo K, Martín-Villalba A. Single-cell transcriptomics reveals a population of dormant neural stem cells that become activated upon brain injury. *Cell Stem Cell*. 2015;17(3):329-340.
 46. Bragado Alonso S, Reinert JK, Marichal N, et al. An increase in neural stem cells and olfactory bulb adult neurogenesis improves discrimination of highly similar odorants. *EMBO J*. 2019;38(6):1-13.
 47. Shibata T, Yamada K, Watanabe M, et al. Glutamate transporter GLAST is expressed in the radial glia-astrocyte lineage of developing mouse spinal cord. *J Neurosci*. 1997;17(23):9212-9219.
 48. Hartfuss E, Galli R, Heins N, Götz M. Characterization of CNS precursor subtypes and radial glia. *Dev Biol*. 2001;229(1):15-30.
 49. Beckervordersandforth R, Deshpande A, Schaffner I, et al. In vivo targeting of adult neural stem cells in the dentate gyrus by a split-cre approach. *Stem Cell Reports*. 2014;2(2):153-162.
 50. Walker TL, Wierick A, Sykes AM, et al. Prominin-1 allows prospective isolation of neural stem cells from the adult murine hippocampus. *J Neurosci*. 2013;33(7):3010-3024.
 51. Suh H, Consiglio A, Ray J, Sawai T, D'Amour KA, Gage FH. In vivo fate analysis reveals the multipotent and self-renewal capacities of Sox2+ neural stem cells in the adult hippocampus. *Cell Stem Cell*. 2007;1(5):515-528.
 52. Shin J, Berg DA, Zhu Y, et al. Single-cell RNA-Seq with waterfall reveals molecular cascades underlying adult neurogenesis. *Cell Stem Cell*. 2015;17(3):360-372.
 53. Suh H, Zhou QG, Fernandez-Carasa I, et al. Long-term labeling of hippocampal neural stem cells by a lentiviral vector. *Front Mol Neurosci*. 2018;11:415.
 54. Dulken BW, Leeman DS, Boutet SC, Hebestreit K, Brunet A. Single-cell transcriptomic analysis defines heterogeneity and transcriptional dynamics in the adult neural stem cell lineage. *Cell Rep*. 2017;18(3):777-790.
 55. Mira H, Morante J. Neurogenesis from embryo to adult - lessons from flies and mice. *Front Cell Dev Biol*. 2020;8:533.
 56. Belenguer G, Duart-Abadia P, Jordan-Pla A, et al. Adult neural stem cells are alerted by systemic inflammation through TNF-alpha receptor signaling. *Cell Stem Cell*. 2021;28(2):285-299.
 57. Ninkovic J, Steiner-Mezzadri A, Jawerka M, et al. The BAF complex interacts with Pax6 in adult neural progenitors to establish a neurogenic cross-regulatory transcriptional network. *Cell Stem Cell*. 2013;13(4):403-418.
 58. Kikkawa T, Casingal CR, Chun SH, et al. The role of Pax6 in brain development and its impact on pathogenesis of autism spectrum disorder. *Brain Res*. 1705;2019:95-103.
 59. Dimou L, Simon C, Kirchhoff F, Takebayashi H, Gotz M. Progeny of Olig2-expressing progenitors in the gray and white matter of the adult mouse cerebral cortex. *J Neurosci*. 2008;28(41):10434-10442.
 60. Gleeson JG, Lin PT, Flanagan LA, Walsh CA. Doublecortin is a microtubule-associated protein and is expressed widely by migrating neurons. *Neuron*. 1999;23(2):257-271.
 61. Weigmann A, Corbeil D, Hellwig A, Huttner WB. Prominin, a novel microvilli-specific polytopic membrane protein of the apical surface of epithelial cells, is targeted to plasmalemmal protrusions of non-epithelial cells. *Proc Natl Acad Sci USA*. 1997;94(23):12425-12430.
 62. Méndez-Gómez HR, Vergaño-Vera E, Abad JL, et al. The T-box brain 1 (Tbr1) transcription factor inhibits astrocyte formation in the olfactory bulb and regulates neural stem cell fate. *Mol Cell Neurosci*. 2011;46(1):108-121.
 63. Mullen RJ, Buck CR, Smith AM. NeuN, a neuronal specific nuclear protein in vertebrates. *Development*. 1992;116(1):201-211.
 64. Su X, Vasilkovska T, Frohlich N, et al. Characterization of cell type-specific S100B expression in the mouse olfactory bulb. *Cell Calcium*. 2021;94:102334.
 65. Kohwi M, Petryniak MA, Long JE, et al. A subpopulation of olfactory bulb GABAergic interneurons is derived from Emx1- and Dlx5/6--expressing progenitors. *J Neurosci*. 2007;27(26):6878-6891.
 66. Young KM, Fogarty M, Kessaris N, Richardson WD. Subventricular zone stem cells are heterogeneous with respect to their embryonic origins and neurogenic fates in the adult olfactory bulb. *J Neurosci*. 2007;27(31):8286-8296.
 67. Winpenny E, Lebel-Potter M, Fernandez ME, et al. Sequential generation of olfactory bulb glutamatergic neurons by Neurog2-expressing precursor cells. *Neural Dev*. 2011;6:12.
 68. Azim K, Hurtado-Chong A, Fischer B, et al. Transcriptional hallmarks of heterogeneous neural stem cell niches of the subventricular zone. *STEM CELLS*. 2015;33(7):2232-2242.
 69. Yang Z. Postnatal subventricular zone progenitors give rise not only to granular and periglomerular interneurons but also to interneurons in the external plexiform layer of the rat olfactory bulb. *J Comp Neurol*. 2008;506(2):347-358.
 70. Bito H, Deisseroth K, Tsien RW. CREB phosphorylation and dephosphorylation: a ca(2+)- and stimulus duration-dependent switch for hippocampal gene expression. *Cell*. 1996;87(7):1203-1214.
 71. Benito E, Barco A. The neuronal activity-driven transcriptome. *Mol Neurobiol*. 2015;51(3):1071-1088.
 72. Vicario-Abejón C, Owens D, McKay R, Segal M. Role of neurotrophins in central synapse formation and stabilization. *Nat Rev Neurosci*. 2002;3(12):965-974.
 73. Crespo C, Liberia T, Blasco-Ibanez JM, et al. The circuits of the olfactory bulb. The exception as a rule. *Anat Rec*. 2013;296(9):1401-1412.
 74. Lee DA, Bedont JL, Pak T, et al. Tanycytes of the hypothalamic median eminence form a diet-responsive neurogenic niche. *Nat Neurosci*. 2012;15(5):700-702.
 75. Álvarez-Buylla A, Kohwi M, Nguyen TM, et al. The heterogeneity of adult neural stem cells and the emerging complexity of their niche. *Cold Spring Harb Symp Quant Biol*. 2008;73:357-365.

76. Fuentealba LC, Rompani SB, Parraguez JI, et al. Embryonic origin of postnatal neural stem cells. *Cell*. 2015;161(7):1644-1655.
77. Whitman MC, Greer CA. Synaptic integration of adult-generated olfactory bulb granule cells: basal axodendritic centrifugal input precedes apical dendrodendritic local circuits. *J Neurosci*. 2007;27(37):9951-9961.
78. Sanai N, Nguyen T, Ihrie RA, et al. Corridors of migrating neurons in the human brain and their decline during infancy. *Nature*. 2011;478(7369):382-386.
79. Bergmann O, Liebl J, Bernard S, et al. The age of olfactory bulb neurons in humans. *Neuron*. 2012;74(4):634-639.
80. Huart C, Rombaux P, Hummel T. Neural plasticity in developing and adult olfactory pathways - focus on the human olfactory bulb. *J Bioenerg Biomembr*. 2019;51(1):77-87.
81. Lazarini F, Lledo PM. Is adult neurogenesis essential for olfaction? *Trends Neurosci*. 2011;34(1):20-30.
82. Lazarini F, Gabellec MM, Torquet N, Lledo PM. Early activation of microglia triggers long-lasting impairment of adult neurogenesis in the olfactory bulb. *J Neurosci*. 2012;32(11):3652-3664.
83. Brann DH, Tsukahara T, Weinreb C, et al. Non-neuronal expression of SARS-CoV-2 entry genes in the olfactory system suggests mechanisms underlying COVID-19-associated anosmia. *Sci Adv*. 2020;6(31):1-19.
84. Bilinska K, Jakubowska P, Von Bartheld CS, et al. Expression of the SARS-CoV-2 entry proteins, ACE2 and TMPRSS2, in cells of the olfactory epithelium: identification of cell types and trends with age. *ACS Chem Neurosci*. 2020;11(11):1555-1562.
85. Meinhardt J, Radke J, Dittmayer C, et al. Olfactory transmucosal SARS-CoV-2 invasion as a port of central nervous system entry in individuals with COVID-19. *Nat Neurosci*. 2021;24(2):168-175.
86. Niesen M, Trotta N, Noel A, et al. Structural and metabolic brain abnormalities in COVID-19 patients with sudden loss of smell. *Eur J Nucl Med Mol Imaging*. 2021:1-12.
87. Christie KJ, Turnley AM. Regulation of endogenous neural stem/progenitor cells for neural repair-factors that promote neurogenesis and gliogenesis in the normal and damaged brain. *Front Cell Neurosci*. 2012;6:70.

SUPPORTING INFORMATION

Additional supporting information may be found online in the Supporting Information section at the end of this article.

How to cite this article: Defteralı Ç, Moreno-Estellés M, Crespo C, et al. Neural stem cells in the adult olfactory bulb core generate mature neurons in vivo. *Stem Cells*. 2021;39(9):1253-1269. <https://doi.org/10.1002/stem.3393>